Metrol. Meas. Syst., Vol. 30 (2023) No. 4, pp. 655–673
DOI: 10.24425/mms.2023.147952

PAN POLSKA AKADEMIA NAUK

METROLOGY AND MEASUREMENT SYSTEMS
Index 330930, ISSN 0860-8229
www.metrology.wat.edu.pl

M&MS

GEAR INVOLUTE ARTIFACTS WITH SUB-MICRON PROFILE FORM DEVIATIONS: MANUFACTURE AND NEW DESIGN

Ming Ling[1)], Siying Ling[2)], Dianqing Yu[3)], Zhihao Zhang[1)], Fengtao Wang[2)], Liding Wang[1)]

1) Key Laboratory for Micro/Nano Technology and System of Liaoning Province, Dalian University of Technology, Dalian 116024, China (*lingming@mail.dlut.edu.cn, 501666391@mail.dlut.edu.cn, wangld@dlut.edu.cn*)
2) Key Laboratory of Intelligent Manufacturing Technology of the Ministry of Education, Shantou University, Shantou 515063, China (✉ *luckling168@163.com, ftwang@stu.edu.cn*)
3) Liaoning Inspection, Examination & Certification Centre, Shenyang 110004, China (*yudianqing@163.com*)

Abstract

Gear involute artifact (GIA) is a kind of calibration standard used for traceability of involute metrology. To machine GIAs with sub-micron profile form deviations, the effect on the involute profile deviations caused by the geometric deviations and 6-DoF errors of the machining tool based on the double roller-guide involute rolling generation mechanism was analysed. At the same time, a double roller-guide involute lapping instrument and a lapping method for GIAs was proposed for lapping and in-situ measuring the gear involute artifacts. Moreover, a new GIA with three design base radii (50 mm, 100 mm, and 131 mm) was proposed for more efficient calibration and was machined with profile form deviations of 0.3 µm (within evaluation length of 38 mm, 68 mm, 80 mm, respectively, measured by the Chinese National Institute of Metrology), and the surface roughness *Ra* of the involute flanks was less than 0.05 µm. The research supports small-batch manufacturing for high-precision GIAs.

Keywords: gear involute artifact, profile deviation, gear standard, involute metrology, gear metrology.

1. Introduction

Gear involute artifact (GIA) is a kind of calibration standard used for traceability of involute metrology. It is mainly used to trace the parameter values of the involute profile and calibrate the *gear measuring instruments* (GMIs) such as gear measuring centres or coordinate measuring machines by comparing the involute profile on GIAs with the involute reproduced by GMIs. GIAs with minimum profile form deviations are used to identify local errors on GMIs, and GIAs with large profile form deviations are used to perform functional tests on GMIs. It is recommended that GIAs be manufactured with deviations less than class-5 in accordance with ISO 1328-1, and with a measurement surface roughness of 0.4 µm *Ra* or better [1, 2].

Article history: received April 19, 2023; revised June 27, 2023; accepted July 2, 2023; available online November 16, 2023.

To ensure the reliability of measurement results between different countries, several measurement comparisons for GIAs were carried out internationally, usually between national metrology institutes and metrology institutes with similar measurement capabilities. In this paragraph, we present some instances of such cooperation. The National Gear Metrology Laboratory (NGML, UK) in the international comparison project EUROMET [3] provided a GIA with a base circle radius of 100 mm, an evaluation length of 38 mm, and profile form deviations of approx. 0.5 µm on the left and right flanks. The Physikalisch-Technische Bundesanstalt (PTB, Germany) provided a GIA with a base radius of approx. 25 mm and a profile form deviation of approx. 0.8 µm within an evaluation length of 17 mm in the international comparison project EURAMT.L-S24 [4]. PTB [5, 6] has also developed, in cooperation with Hofler and others, a large involute gear segment measurement standard with base radii of approx. 470 mm and a large gear ring measurement standard with base radii of approx. 940 mm, the profile form deviations of approx. 2 µm within the evaluation lengths of approx. 120 mm and 84 mm respectively. The Belarusian State Institute of Metrology (BelGIM, Belarus) provided a GIA with two base circles (base radii of 60.140 mm and 150.030 mm, respectively), evaluation lengths of approx. 19 mm and 41 mm, and profile form deviations of approx. 1.8 µm and 0.5 µm in the international comparison project COOMT.L-S10 [7]. In the international comparison project COOMT.L-S18 [8], the National Scientific Centre of Ukraine (NSC, Ukraine) also provided a GIA with two base circles. The structure of the GIA was the same as that provided by BelGIM, with base radii of 60 mm and 150 mm, evaluation lengths of approx. 28 mm and 32 mm, and profile form deviations of approx. 0.9 µm and 4.0 µm respectively. Kyoto University and the National Metrology Institute of Japan (NMIJ, Japan) [9] have developed a double roller-guide involute reference instrument based on laser measurement. The GIA used for the measurement experiments has a base radius of 57.5 mm, with an evaluation length of approx. 20 mm, and a profile form deviation of approx. 0.5 µm, OSAKA SEIMITSU KIKAI CO., LTD (OSK, Japan) [10], in the process of developing a high precision GMI, provided a GIA with a base radius of 100 mm, an evaluation length of approx. 29 mm and profile form deviations of approx. 0.5 µm on the left and right flanks which was used to verify the measurement precision of the GMI. Ling *et al.* [11] machined a class-1 involute cylindrical standard gear with a base radius of approx. 56 mm, an evaluation length of approx. 20 mm, and a profile form deviation of approx. 1.3 µm. The GIAs above represent the leading level of involute machining in each country.

To further improve the machining accuracy of GIAs and to obtain small batch manufacturing of GIAs with sub-micron profile form deviations, a double roller-guide involute rolling generation mechanism was used to machine and measure GIAs in this paper. In Section 2, the rolling generation method of the involute machining was described and the effect on the involute profile deviations caused by the errors of the machining tool was analysed. In Section 3, a lapping instrument for a GIA based on a double roller-guide involute rolling generation mechanism was designed for the lapping and in-situ measurement of the involute profile.

In addition, when using GIAs to evaluate the measurement errors of GMIs, multiple GIAs with different base radii are usually required to cover a wide measurement range of the calibrated instrument and to ensure the value stability of GIAs [1, 2]. Although the GIAs used in COOMT.L-S10 and L-S18 have two base radii, the differences in profile form deviations between the flanks of two base radii were 3 to 4 times and the gravity centres of GIAs were off the central axis of the mandrels, which may increase the error of the rotary table. The PTB [12] has also developed a GIA that incorporates multiple internal flanks, but has a tip diameter of 20 mm and normal modules of 0.1 mm, 0.2 mm, 0.5 mm, and 1 mm respectively. It was mainly used for the calibrations of GMIs with small gear measurement.

Therefore, in Section 4, a new GIA with three base radii was proposed for more efficient calibration, and Section 5 reports this GIA was machined and measured using the instrument designed in this paper and measurements including those performed by the Chinese National Institute of Metrology (NIM, China) were carried out.

2. Effect on involute profile deviations caused by errors of the machining tool

2.1. Effect on involute profile deviations caused by 6-DoF errors of the machining tool

As a line (generating line) rolling along a fixed circle (base circle), the track generated by a fixed point on the line is called the involute of the base circle, which is the principle of involute rolling generation. The principle of machining an involute by double roller-guide rolling generation mechanism is shown in Fig. 1(a). As the rollers roll on the guide, the intersection point P of the standard involute and the generating line (guide) is a fixed point, and the base radius of the standard involute is the same as the roller radius. So, a machining tool can be arranged at point P (usually a cup or butterfly grinding wheel when grinding) to machine the involute, and a probe can be arranged at point P to measure the involute as shown in Fig. 1(b). This roller-guide involute rolling-generation method is in line with the principle of involute generation, with a simple mechanism and few error sources. Takeoka and Lou *et al.* [9–13] developed the involute measuring instruments with measurement uncertainties U_{95} not more than 0.5 µm on the part of the double roller-guide involute rolling generation mechanism. Therefore, this rolling generation method has the possibility of machining a high-precision involute.

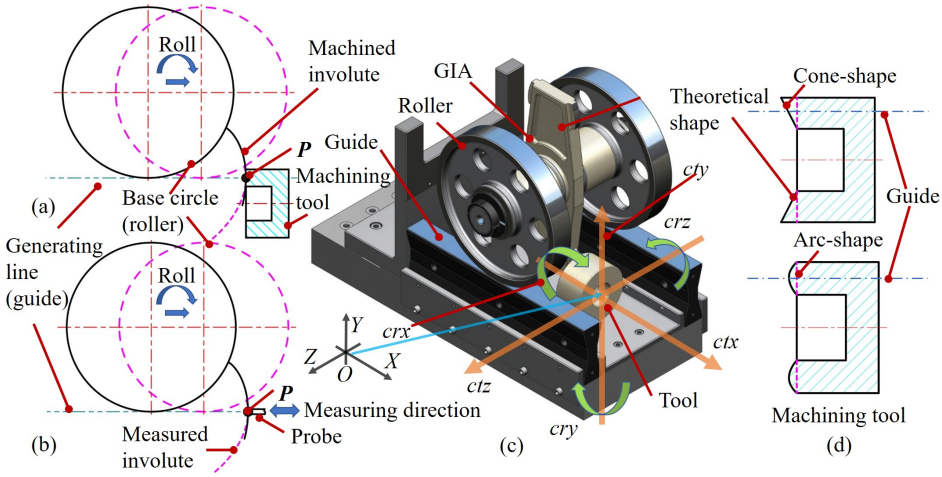

Fig. 1. Involute machining and measurement based on rolling generation and errors of the machining tool: (a) Involute machining based on rolling generation; (b) Involute measurement based on rolling generation; (c) 6-DoF errors of the machining tool; (d) Geometric deviations of workface of machining tool.

The contact area between the machining tool and the machined involute flank is a section of the area involved in meshing during generating grinding such as worm gear grinding, large plane grinding, *etc*. The grinding wheel involved in grinding is the opposite profile to the machined involute flank during profile grinding. But the grinding wheel during rolling generation grinding is only in contact with the machined involute flank at point P, so the requirements of dressing

for the grinding wheel are significantly reduced compared to other tooth grinding methods, and errors in the grinding wheel system are less likely to be reflected on the involute flanks.

The workface of the machining tool is perpendicular to the generating line (workface of guide) in theory, but in the actual machining, the workface of the machining tool is difficult to be ideal plane perpendicular to the guide plane caused by the rotation error, feeding error, dressing error of the machining tool and so on as shown in Fig. 1(d). The effect of 6-DoF errors of the machining tool on the involute profile deviations was considered below, taking grinding as an example.

In the 6-DoF errors of the grinding wheel system as shown in Fig. 1(c), the *XOZ*-plane is the workface of guides, the *X*-axis is along the direction of the tool feed, the *Y*-axis is normal to the workface of guides, the *Z*-axis is along the direction of the theoretical centre axis of GIA and the point *O* is the theoretical contact point between the middle section of the GIA and the machining tool (point *P* in Fig. 1). During grinding, *crx* is the rotation of the grinding wheel, and the *crx* error can be negligible. The *ctx* is the feeding direction of the grinding wheel and the direction of axial runout of the grinding wheel, and the *ctx* error affects the involute profile deviations directly. This error was discussed in detail in Subsection 2.2. The *cty* and *ctz* are the radial runout of the grinding wheel along the *X* and *Z*-axis, and the *cty* and *ctz* errors do not affect the involute machining. The *crz* is the rotation of the grinding wheel around the *Z*-axis, which makes an angle between the workface of the grinding wheel and the generating line (workface of the guide).

This error has some similarities to dressing the grinding wheel to a cone-shape (as shown in Fig. 1(d)), and the effect of *crz* error and slope deviation of the machining tool on profile deviations was discussed in Subsection 2.3.

The *cry* is the rotation of the grinding wheel around the *Y*-axis, which mainly causes the helix deviations (the helix deviations are not regarded as the evaluation items for GIAs generally). The actual involute at the mid-section of the tooth flank is still the standard involute, but there is a collision volume of the stylus when measuring GIAs, so the actual contact points between the stylus and the measured flank may not be at the mid-section of the tooth flank, which will affect the results of the involute measurement. At this point, the measured profile deviation f_i (distance of the actual involute from the standard involute) satisfies:

$$f_i = r_{\text{probe}} \left(\frac{1}{\cos \theta_{cryi}} - 1 \right), \tag{1}$$

where r_{probe} is the stylus radius of the probe, θ_{cryi} is the angle of *cry* at rolling angle θ_i.

The mean profile line is fitted with the least square method [14]:

$$f_i' = k\theta_i + c, \qquad k = \frac{\overline{\theta_i f_i} - \overline{\theta_i}\,\overline{f_i}}{\overline{\theta_i^2} - \left(\overline{\theta_i}\right)^2}, \qquad c = \overline{f_i} - k\overline{\theta_i}\,. \tag{2}$$

The profile slope deviation $f_{H\alpha}$ is the distance between two facsimiles of the standard profile which intersect the extrapolated mean profile line at the profile control diameter and the tip diameter [14], which satisfies:

$$f_{H\alpha} = \frac{kL_\alpha}{r_b}, \tag{3}$$

where L_α is the evaluation length and r_b is the theoretical base radius. And the profile slope deviation can be compensated to the actual base radius r_{bs} of the involute with the following equation:

$$r_{bs} = r_b \left(\frac{f_{H\alpha}}{L_\alpha} + 1 \right). \tag{4}$$

Metrol. Meas. Syst., Vol. 30 (2023), No. 4, pp. 655–673
DOI: 10.24425/mms.2023.147952

The profile form deviation $f_{f\alpha}$ is the distance between two facsimiles of the mean profile line which encloses the measured profile over the profile evaluation range [14], which satisfies:

$$f_{f\alpha} = \max\left(f_i - f_i'\right) - \min\left(f_i - f_i'\right). \tag{5}$$

It can satisfy $|\theta_{cryi}| < 0.01°$ during grinding, thus the effect on profile form deviations caused by the *cry* error is only a few nanometres and can be neglected.

The *ctx* error, *crz* error and the geometric deviations (slope and form deviations) of the machining tool were analysed below. The profile slope deviation of a GIA needs to be compensated to the base radius in use, so mainly the effect on profile form deviation was considered in this paper.

2.2. Effect on involute profile deviations caused by ctx error of the machining tool

Firstly, the effect on the profile deviations caused by the *ctx* error was considered. To facilitate the analysis, the motion of the base circle rolling and the machining tool fixed in Fig. 1 was transformed into the motion of the base circle fixed and the machining tool rolling as shown in Fig. 2. The centre of the base circle is the origin-O, and the line between the start of the involute at the base circle and the origin-O is the X-axis to establish a Cartesian coordinate system.

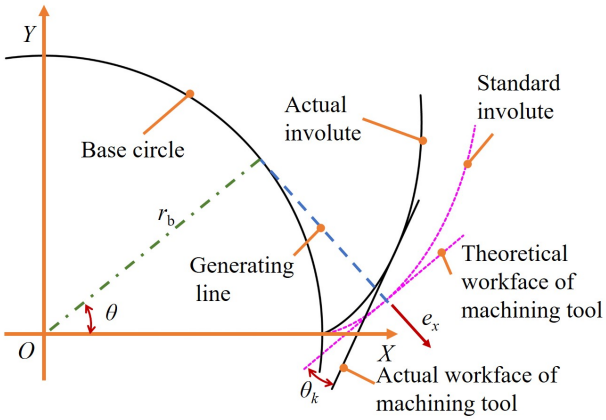

Fig. 2. Effect on the involute profile caused by the error of the machining tool.

The workface of the machining tool was considered a continuous surface without considering the effect of the grit size. The actual involute satisfies:

$$\begin{cases} x_{Le1} = r_b \cos\theta + (r_b\theta + e_x)\sin\theta \\ y_{Le1} = r_b \sin\theta - (r_b\theta + e_x)\cos\theta \end{cases}. \tag{6}$$

The rolling angle θ_L on the standard involute corresponding to the actual involute is:

$$\theta_L = \arccos\frac{r_b}{\sqrt{x_{Le1}^2 + y_{Le1}^2}} + \arcsin\frac{y_{Le1}}{\sqrt{x_{Le1}^2 + y_{Le1}^2}}. \tag{7}$$

The corresponding point (x_L, y_L) on the standard involute at rolling angle θ_L satisfies:

$$\begin{cases} x_L = r_b \cos\theta_L + r_b\theta_L \sin\theta_L \\ y_L = r_b \sin\theta_L - r_b\theta_L \cos\theta_L \end{cases}. \tag{8}$$

The corresponding point (x_P, y_P) on the base circle at rolling angle θ_L satisfies:

$$\begin{cases} x_P = r_b \cos\theta_L \\ y_P = r_b \sin\theta_L \end{cases}. \tag{9}$$

The profile deviation f_i satisfies:

$$f_i = \sqrt{(x_{Le1} - x_P)^2 + (y_{Le1} - y_P)^2} - \sqrt{(x_L - x_P)^2 + (y_L - y_P)^2}. \tag{10}$$

The grinding wheel needs to be statically and dynamically balanced on the grinding wheel spindle before grinding, and be thermally balanced for a period before high-precision grinding (more than 3 hours generally), at this point $|e_x| < 0.5$ µm generally. The e_x error can be regarded as a normal distribution error or a uniform distribution error. So, the uniform distribution error was as taken an example below, the involute with base radius $r_b = 100$ mm and evaluation range in roll path length of 5 mm–65 mm. The profile deviations caused by the e_x error were shown in Fig. 3, the e_x error is be mapped approximately 1:1 to the profile form deviations, the effect on the profile slope deviations was approx. 5% e_x. Therefore, the e_x error must be minimised to obtain GIAs with sub-micron profile form deviations.

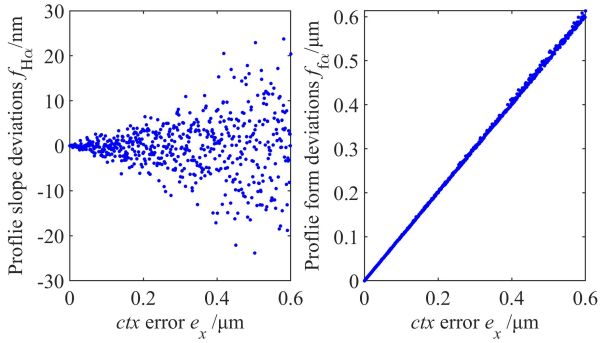

Fig. 3. Simulation of profile deviations caused by the *ctx* error of the machining tool.

2.3. Effect on involute profile deviations caused by slope deviation and crz error of the machining tool

The workface of the machining tool is easily dressed to a cone-shape rotating around the Z-axis as shown in the upper right diagram in Fig. 1(d). The angle between the actual and theoretical workface of the machining tool was noted as tool angle θ_k as shown in Fig. 2, which is positive counter clockwise. The initial workface of the machining tool at rolling angle $\theta = 0°$ satisfies:

$$y_0 = x_0 \tan\theta_k + b. \tag{11}$$

Metrol. Meas. Syst., Vol. 30 (2023), No. 4, pp. 655–673
DOI: 10.24425/mms.2023.147952

The workface of the machining tool at rolling angle θ is:

$$\begin{bmatrix} x \\ y \end{bmatrix} = \begin{bmatrix} \cos\theta & -\sin\theta \\ \sin\theta & \cos\theta \end{bmatrix} \begin{bmatrix} x_0 & 0 \\ y_0 & -r_b\theta \end{bmatrix}. \tag{12}$$

The curve family of the workface of the machining tool after eliminating x_0 is:

$$y = \frac{(\sin\theta + \tan\theta_k \cos\theta)x + b - r_b\theta}{\cos\theta - \tan\theta_k \sin\theta}. \tag{13}$$

The discriminant equation for the curve family satisfies:

$$\frac{\partial y}{\partial \theta} = \left(1 + \tan^2\theta_k\right) x - r_b\left(\cos\theta - \tan\theta_k \sin\theta\right) + (b - r_b\theta)\left(\sin\theta + \tan\theta_k \cos\theta\right) = 0. \tag{14}$$

So, the actual machined involute satisfies:

$$\begin{bmatrix} x_{Le2} \\ y_{Le2} \end{bmatrix} = \frac{1}{1 + \tan^2\theta_k} \begin{bmatrix} \cos\theta & -\tan\theta_k \sin\theta \\ \sin\theta & \tan\theta_k \cos\theta \end{bmatrix} \begin{bmatrix} r_b \\ b - r_b\theta \end{bmatrix}. \tag{15}$$

The value of C mainly affects the phase of involute relative to the centre of the base circle. In the case of the involute shown in Fig. 2, the value of C takes:

$$b = -r_b \tan\theta_k. \tag{16}$$

The profile deviations can be calculated by substituting (7) into (2). Considering first the case where θ_k was a constant, the involute with base radius r_b = 100 mm and evaluation range in the roll path length of 5 mm – 65 mm was an example. The profile deviations caused by the slope deviation of the workface of the machining tool were shown in Fig. 4, the slope deviation mainly affects the profile slope deviations of the machined involute, and the effect on the profile form deviations can be ignored.

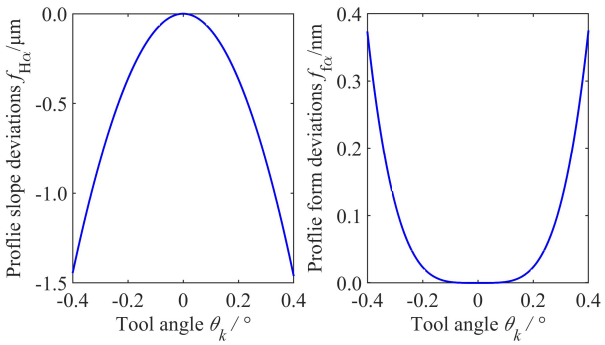

Fig. 4. Simulation of profile deviations caused by the slope deviation of the machining tool.

It should be noted that if the involute is still machined according to the design roll path length as the workface of the machining tool is sloping, it will result in root cutting or incomplete machining at the root of the machined involute. The affected rolling angle θ_{ke} satisfies:

$$\begin{cases} \theta_{ke} = \theta_k, & \theta_k > 0 \\ \sin(\theta_k - \theta_{ke}) + \theta_{ke}\cos(\theta_k - \theta_{ke}) = \theta_k, & \theta_k < 0 \end{cases}. \tag{17}$$

Equation (17) can be approximated with the numerical method:

$$\begin{cases} \theta_{ke} = \theta_k, & \theta_k > 0 \\ \theta_{ke} = -\theta_k/2, & \theta_k < 0 \end{cases}. \tag{18}$$

So, the machining tool should be dressed to tool angle $\theta_k < 0$ to avoid the root of the flank not being machined to cause error accumulation. The roll path length to the start of profile evaluation is millimetres generally, therefore, the effect on the profile form deviations caused by the slope deviation of the workface of the machining tool can be negligible.

Then the effect of the *crz* error θ_{crz} on the involute profile deviations was considered below. It was assumed that the *crz* error is random, while the *crz* error is periodic, the effect on the profile deviations is between the *crz* error being a random error and a constant error. the effect of the *crz* error on the profile deviation was shown in Fig. 5. The *crz* error is mainly related to the motion accuracy of the spindle system. It is easy to obtain the accuracy of $|\theta_{crz}| < 0.01°$ (approx. 17 µm/100 mm), which also has a negligible effect on profile deviation.

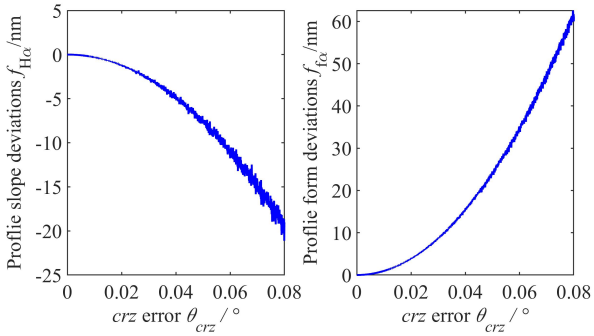

Fig. 5. Simulation of profile deviations caused by the *crz* error of the machining tool.

2.4. Effect on involute profile deviations caused by form deviation of the machining tool

On the other hand, the workface of the machining tool cannot be dressed to an ideal plane. The form deviation of the workface of the machining tool was treated as an arc in this paper, as shown in the lower right-hand diagram in Fig. 1(d). The centre of the arc is (x_p, y_p) and the arc radius is r_p. The initial workface at rolling angle $\theta = 0°$ is:

$$\begin{cases} x_0 = x_p + r_p \cos t \\ y_0 = y_p + r_p \sin t \end{cases}. \tag{19}$$

The curve family of the workface of the machining tool after rolling generation also satisfies (11), and the discriminant equation is:

$$\frac{\partial x}{\partial t}\frac{\partial y}{\partial \theta} - \frac{\partial x}{\partial \theta}\frac{\partial y}{\partial t} = (r_b - x_p)\sin t - (r_b\theta - y_p)\cos t = 0, \tag{20}$$

where

$$\begin{cases} \sin t = \dfrac{r_b\theta - y_p}{\sqrt{(r_b\theta - y_p)^2 + (r_b - x_p)^2}} \\ \cos t = \dfrac{r_b - x_p}{\sqrt{(r_b\theta - y_p)^2 + (r_b - x_p)^2}} \end{cases}. \tag{21}$$

Metrol. Meas. Syst., Vol. 30 (2023), No. 4, pp. 655–673
DOI: 10.24425/mms.2023.147952

When the workface of the machining tool has a form deviation and the tip of the workface in the *XOY*-plane is in the workface of the guide (the tip of the arc is at point *P*), and when the grinding wheel is convex at point *P*, it can be regarded as a large stylus of the probe in contact with the tooth flank, which does not affect the involute machining. When the tip of the workface in the *XOY*-plane is not in the workface of the guide (the tip of the arc is not at point *P*), the contact point between the workface and tooth flank is no longer just point *P*, but will also become an area on the workface, similar to that when the workface is sloping or the probe has a positioning error. There is an effect on the profile slope deviation, but it can be ignored as shown in Fig. 6.

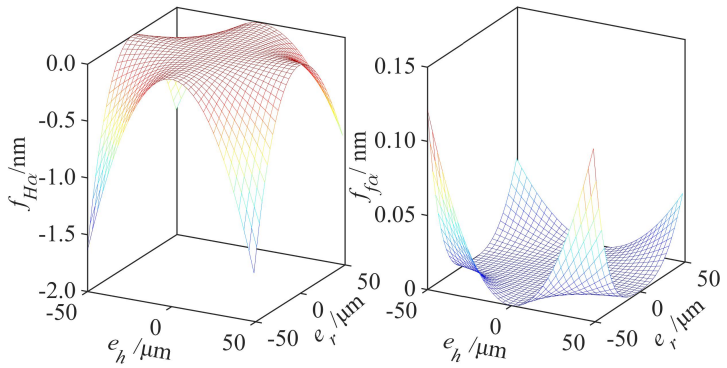

Fig. 6. Simulation of profile deviations caused by the form deviation of the workface of the machining tool. $f_{H\alpha}$ is the profile slope deviation, $f_{f\alpha}$ is the profile form deviation, e_r is the distance that the arc vertex deviates from the generating line (guide plane), and e_h is the chord height for a chord length of 10 mm.

The situation is special when the grinding wheel is concave. If the curvature radius of the workface is greater than the roll path length of the tip of the involute in the contact area between the workface and tooth flank, the effect on the profile form deviation can be in this case negligible , as shown in Fig. 6. But as the machining tool wears, the curvature radius of the workface may be smaller than the roll path length of the tip of the involute in the contact area between the machining tool and tooth flank, then the edge of the micro-pit of the machining tool may participate in machining. That will cause the root of the involute not to be machined and the tip of the involute to be over-machined and easily cause burns when grinding, not only reducing the machining accuracy of the involute but also reducing the hardness of the burned area and retaining greater residual stress and heat, which is detrimental to the quantitative stability of a GIA. Therefore, the dressing frequency for the machining tool should be appropriately increased to avoid this situation as much as possible.

3. Lapping method for the GIA

3.1. Double roller-guide involute lapping instrument

As shown in the previous section, the *ctx* error of the machining tool is the main error source in the profile form deviation, which is mainly the axial runout error. The axial runout error can be reduced by using electric spindles or air-bearing spindles. Also, better grinding properties can be achieved by a structured grinding wheel [15] or an elastic bonded grinding wheel [16]. Condition monitoring of the grinding wheel [17] for the timely dressing of the grinding wheel also facilitates better profile deviations. And the profile deviations due to the axial runout error during grinding

can be reduced by optimizing the spindle speed of the grinding wheel and the rolling speed of the rollers. But the axial runout of the grinding wheel, the grinding heat, and the residual stress are not easily eliminated, which is detrimental to the machining of GIAs with sub-micron profile form deviations.

Moreover, the GIA, as a kind of measurement standard, has high requirements for dimensional stability. Therefore, instead of optimization in grinding, an involute lapping instrument for GIA based on rolling generation was proposed, as shown in Fig. 7. In this way, the rotational grinding wheel was replaced with a stationary whetstone, so there was no axial runout. Furthermore, the dressing of the whetstone was much easier than that of the grinding wheel, and the dressing accuracy of the whetstone was much higher easy to achieve. The machined flank is also less susceptible to the effects caused by grinding heat and residual stress. So, the lapping method has more potential to obtain an involute flank with better profile form deviation, surface roughness and dimensional stability.

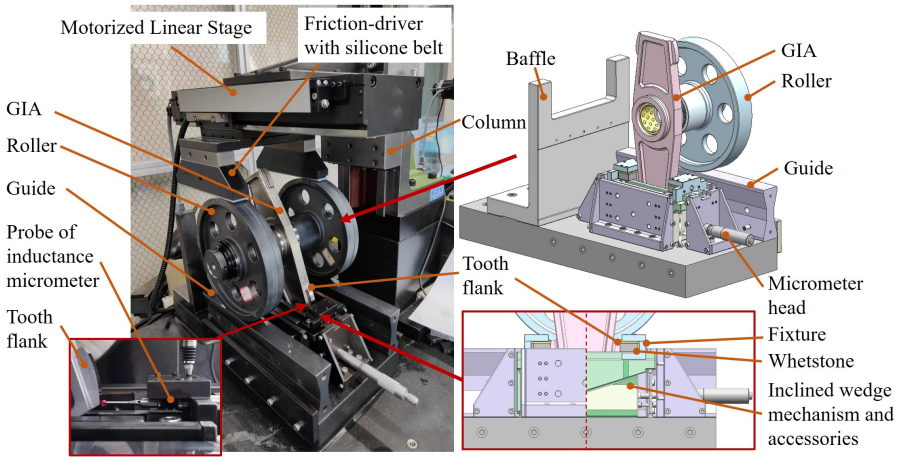

Fig. 7. Double roller-guide involute lapping instrument based on rolling generation.

The assembled component of rollers and the GIA rolled on the guides, which were driven by a motorized linear stage with a silica gel plate or polyurethane plate. And the involute flank was lapped by a whetstone sintered most often with Boron Carbide (B_4C) or Silicon Carbide (SiC). The surface of the B_4C whetstone is usually more porous allowing for higher lapping efficiency, while the denser surface of the SiC whetstone allows for lower surface roughness after lapping. The whetstone was held by a fixture. Moreover, the GIA can be measured in-situ by removing the whetstone and replacing it with a probe. A TESA inductance micrometer (a GT21HP high precision probe and a TT80 electronic length measuring instrument) was used to measure the involute profile with a measurement uncertainty of $U_{95} = (0.07 + 0.4L)$ µm (L is the measured length in mm). The positioning method of the probe can be found in [18].

The wedge angle was retained between the workface of the whetstone and the workface of the guide, and the perpendicular deviation was 0.5 µm/mm–1 µm/mm. The feeding motion of the micrometer head in the horizontal direction was converted into the displacement of the whetstone in the vertical direction by the inclined wedge mechanism and accessories to avoid overuse of the whetstone in the same position and to achieve micro-feeding during lapping (tens of nanometres per scale of the micrometer head).

Moreover, the lapping can change the surface texture of the tooth flank. After grinding, the surface texture is usually along the direction of facewidth, while the surface texture is along the direction of involute after lapping, which is more favourable for the use of GIAs.

3.2. Lapping for a GIA with area-by-area removal

To improve lapping efficiency, a lapping method called "area-by-area removal" was proposed, which process is shown in Fig. 8. The GIA was machined with gear grinding machines or wire-cutting machines to fulfil the specifications of the evaluation range and the profile form deviations were less than 3 µm before lapping. First, the GIA was measured in-situ to obtain the profile deviations of the machined flank. The mean profile line and profile form deviation were obtained, and the relatively high area (the portion of the profile deviations above the mean profile line) was identified. The pre-lapped area was the between 70% and 80% of the area between a_i and b_i with a pre-lapping removal of (30%–40%)$f_{f\alpha}$.

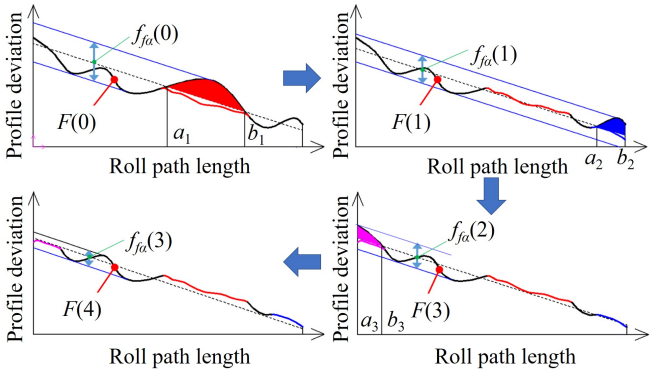

Fig. 8. Schematic of lapping for GIA with area-by-area removal.

Following that, it was roughly lapped. The workface of the B_4C whetstone was first lapped to a flatness error of less than 1 µm, and then the workface of the whetstone was roughened to obtain a larger lapping removal. After the profile form deviation $f_{f\alpha}$ was less than 0.5 µm, the entire flank was lapped with the SiC whetstone to reduce the profile form deviation and surface roughness even further. Finally, the tooth flank was polished with polishing solutions after a polishing pad was applied to the whetstone.

4. New GIA with three design base circles

When using GIAs to calibrate GMIs for the measurement accuracy, repeatability and reproducibility of involute profile deviations, the minimum requirement is that the GIA should be selected as near as practical to the centre of the measurement range over which the GMI is used. Ideally, the geometry of GIAs should represent the parameters of the product gears or be with multiple base radii as far as possible to cover the widest possible measuring range of GMIs [1, 2]. In China, when calibrating GMIs with GIAs the calibration laboratories trace the involute parameters, the used GIAs must have three different base radii, with the difference between the maximum and minimum base radius being 80 mm or more [19]. To meet these requirements,

and improve the calibration efficiency, a new GIA with three design base radii was proposed, as shown in Fig. 9, and the design parameters were shown in Table 1. This new GIA allows the tracing of involutes with three base radii in a single mounting, which allows for more efficient calibration.

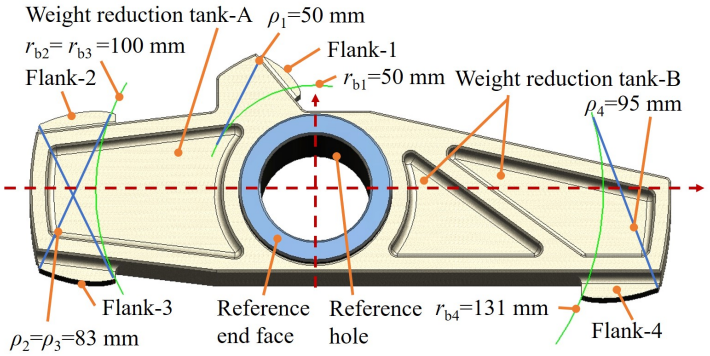

Fig. 9. Structure of a new GIA with three design base circles.

The GIA has four flanks, Flank-1 has a design base radius r_{b1} = 50 mm and roll path length ρ_1 = 0–50 mm, Flank-2 and Flank-3 are the left and right flank with the same design base radii r_{b2} = r_{b3} = 100 mm and roll path lengths ρ_2 = ρ_3 = 0–83 mm, and Flank-4 has a design base radius r_{b4} = 131 mm and roll path length ρ_4 = 0–95 mm. The gravity centre of GIA and the geometric centre of the base circle of the four flanks overlap the axis of the reference hole by adjusting the depth of weight reduction tanks A and B.

Table 1. Design parameters of a GIA with three design base circles.

Flank	**Base radius r_b / mm**	**Tip radius r_a / mm**	**Roll path length ρ / mm**	**Number of teeth* z**	**Normal module* m_n / mm**	**Facewidth b / mm**	**Pressure angle α_n / °**	**Helix angle β / °**
1	50	70.5	49.70161	6	17.73630	8	20	0
2	100	130	83.06624	9	23.64839	8	20	0
3	100	130	83.06624	9	23.64839	8	20	0
4	131	161.8	94.96441	12	23.23455	8	20	0

*The number of teeth and normal modulus of GIA can be changed, and are given to facilitate the input for existing measuring procedures and the standardization of values.

5. Machining and measurement of GIAs

A new GIA with three design base circles was machined an direction of facewidth, and the arithmetic mean was taken as the finald measured with a double roller-guide involute lapping instrument. The material of the gears was B00150 with HRC 60-64.

The stylus sphere used for probing was 3 mm in diameter. The profile was measured in the centre of the flanks. Ten data points were taken per millimetre, approximately equally spaced along the roll path length for measurement. The original measurement data was subjected to

the digital Gaussian 50% type filter, and the profile form filter cut-off was $\lambda_\alpha = 1$ mm [13]. The lab temperature was (20 ± 0.3)°C. The instrument proposed in this paper cannot guarantee that the measuring points were located strictly at the mid-section of each flank of the GIA, so measurements were taken 5 times consecutively near the mid-section at two locations approximately 1 mm apart in the direction of facewidth, and the arithmetic mean was taken as the final measurement result. The curves of profile deviation for one of the measurements on each flank are shown in Figure 10. The final measurement results are shown in Table 2, and the results of each measurement are shown in Table A1.

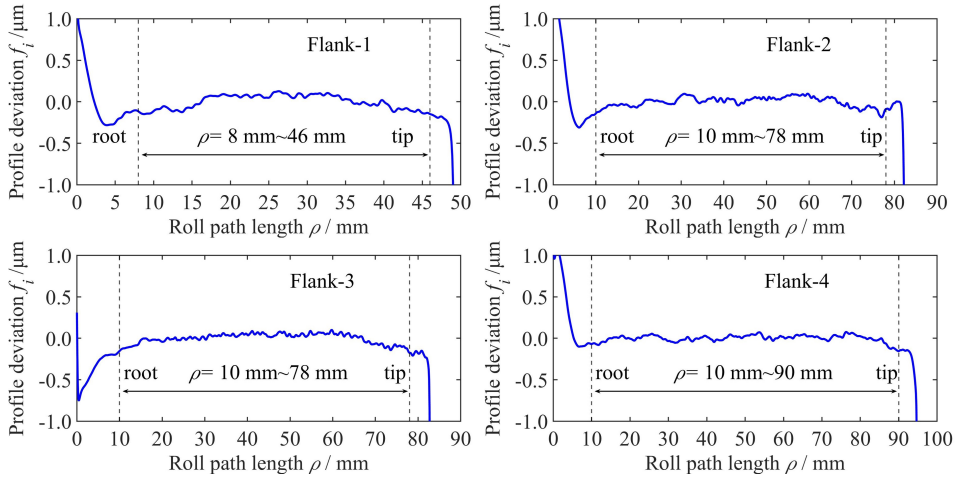

Fig. 10. Curves of profile deviations of the GIA (in-situ measurement, the profile slope deviations corrected to 0).

Table 2. Measurement results of profile form deviations of the GIA.

Flank	Number of teeth z	Normal module* m_n / mm	Evaluation range in roll path length		Profile form deviation $f_{f\alpha}$ / µm	
			Length of roll foot ρ_{start} / mm	Length of roll tip ρ_{end} / mm	In-situ measurement	NIM measurement
1	6	17.73952	8	46	0.23	0.3
2	9	23.64687	10	78	0.30	0.3
3	9	23.64711	10	78	0.28	0.3
4	12	23.23734	10	90	0.22	0.3

*Normal moduli were given by the NIM and have been corrected to make the profile slope deviations of each flank 0.

This GIA was also measured at NIM with a gear involute standard instrument with measurement uncertainty $U(f_{f\alpha}) = 0.8$ µm, $k = 2$ for profile form deviations as shown in Fig. 13. The stylus sphere used for probing was also 3 mm in diameter. The individual flanks were measured with the multi-rotation method (the first measured position of the GIA on the rotary table was recorded as 0° relative to the rotary table, and the GIA was located at 0°, 90°, 180° and 270° relative to the rotary table and measured 2 times respectively.) and the final profile form deviations were the arithmetic mean of the multi-rotation measurements of each flank. The final measurement results are also shown in Table 2 and the results of each measurement are shown in Table A2.

The measurement results performed at the NIM show that the profile form deviations of the four flanks of this GIA were all 0.3 µm. The profile form deviations of this GIA were reduced by approximately 40% to 92% compared to GIAs presented in Section 1, and the profile form deviations per roll path length were reduced by approximately 36% to 97%.

The difference between the measurement results of in-situ measurements and the NIM measurements was less than 0.1 µm. Considering that the measurement repeatability of the gear involute standard instrument at the NIM was 0.1 µm when measuring this GIA as shown in Table A2 (also the resolution of profile form deviation of the gear involute standard instrument at the NIM), the measurement results of in-situ measurement were valid. The proposed double roller-guide involute lapping instrument and lapping method enable the manufacture of GIAs with sub-micron profile form deviations.

The surface roughness of the Flank-2 was measured using a Mahr surface measuring station (Marsurf GD 280, $Urel = 2\%$, $k = 2$) with a sample length of $lr = 0.25$ mm and the arithmetic mean of measurement results is shown in Table 3, the results of each measurement are shown in Table A3 (before the lapping) and Table A4 (after the polishing). And as shown in Fig. 11, compared with the ground tooth surface of the GIA, as the lapping proceeds, the striations along the facewidth caused by grinding were gradually replaced by striations along the direction of the involute on the tooth surface, and the surface roughness *Ra* along the involute direction was reduced from approximately 0.11 µm–0.14 µm to approximately 0.05 µm. With further polishing, the tooth surface no longer has obvious striations, and the surface roughness *Ra* along the involute was reduced to approximately 0.02 µm. Moreover, the surface roughness *Ra* along the facewidth was also reduced from approximately 0.04 µm to approximately 0.02 µm with lapping and polishing. The surface roughness *Ra* along the involute at the tooth root was greater than at the middle and tip of the tooth. On the one hand, this may be due to the greater machining errors remaining at the root (as shown in Fig. 10), and on the other hand, the surface roughness may also be influenced by the stylus diameter of the probe and the radius of curvature of the involute surface.

Table 3. Measurement results of tooth surface roundness of Flank-2 (Unit: µm).

Position of measurements	**Before lapping**		**After polishing**	
	Along involute	Along facewidth	Along involute	Along facewidth
Tooth root	0.1433	0.0372	0.0441	0.0149
Tooth middle	0.1108	0.0326	0.0192	0.0173
Tooth tip	0.1153	0.0377	0.0133	0.0254

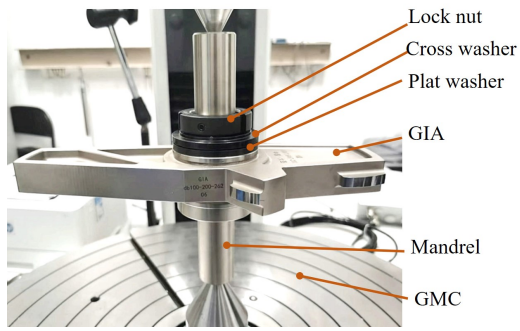

Fig. 11. Measurement of profile form deviations of the GIA with the gear involute standard instrument at the NIM.

Metrol. Meas. Syst., Vol. 30 (2023), No. 4, pp. 655–673
DOI: 10.24425/mms.2023.147952

The accuracy of a GIA can be improved further with this lapping method through improving the accuracy of the rolling generation and probe system as well as a longer lapping time. The GIAs with base radii r_b = 200 mm and 400 mm and sintered ceramic materials will also be intended for machining.

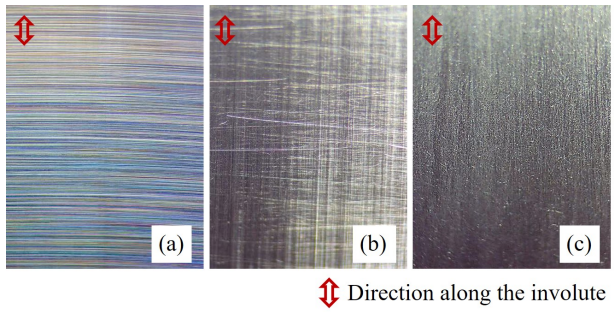

Fig. 12. Surface traces of Flank-2 of a GIA (a) after grinding, (b) after lapping, (c) after polishing.

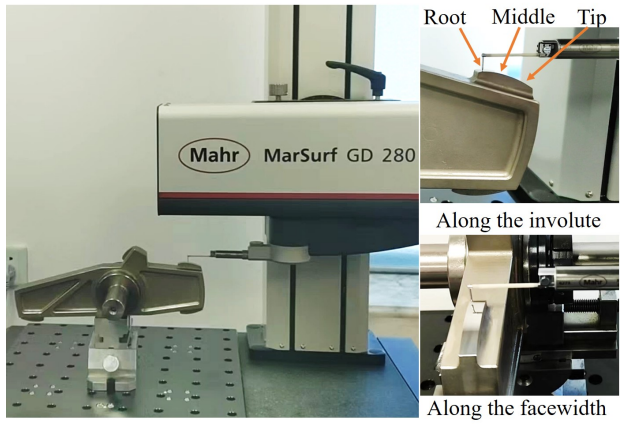

Fig. 13. Measurement for surface roughness of Flank-2 of the GIA.

6. Conclusions

To machine GIAs with sub-micron profile form deviations, this paper analysed the effect on the involute profile deviations caused by geometric deviations and 6-DoF errors in the machining tool system based on the rolling generation. The *ctx* error (usually the axial runout of the machining tool) was identified as the main source of deviation, which is reflected at approximately 1:1 in the profile form deviation.

To address these challenges, a double roller-guide involute lapping instrument was developed to lap and in-situ measure GIAs, and a lapping method known as “area-by-area removal” was proposed to enhance lapping efficiency. Additionally, a new GIA with three designed base radii (50mm, 100mm, and 131mm) was proposed to enable more efficient calibration.

The instrument and methods proposed above make it possible to machine GIAs with profile form deviations of 0.3 μm (measured by the Chinese National Institute of Metrology) and surface roughness *Ra* of involute flanks of less than 0.05 μm.

Overall, this research contributes to the advancement of the small-batch manufacture of GIAs with sub-micron profile form deviations.

Acknowledgements

This work was funded by the National Natural Science Foundation of the People's Republic of China (grant No. 52075067), the STU Scientific Research Initiation (grant No. NTF23008), the Guangdong Provincial University Innovation Team Project (grant No. 2020KCXTD012), and the Fundamental Research Funds for the Central Universities (grant No. DUT22LAB111). The authors would like to thank to the Chinese National Institute of Metrology for the measurements of GIAs.

Appendices

Table A1. Profile form deviations of GIA by in-situ measurement. (Unit: μm)

Flank	Number of measurement										Mean	Standard deviation
	1	2	3	4	5	6	7	8	9	10		
1	0.19	0.21	0.21	0.23	0.17	0.31	0.24	0.21	0.25	0.23	0.23	0.04
2	0.27	0.29	0.26	0.27	0.32	0.33	0.32	0.29	0.31	0.33	0.30	0.03
3	0.31	0.28	0.27	0.31	0.31	0.27	0.29	0.27	0.28	0.25	0.28	0.02
4	0.20	0.23	0.29	0.27	0.20	0.21	0.19	0.17	0.24	0.19	0.22	0.04

Table A2. Profile form deviations of GIA measured by the NIM. (Unit: μm)

Flank	Number of measurement								Mean	Standard deviation
	1	2	3	4	5	6	7	8		
1	0.3	0.3	0.3	0.3	0.3	0.3	0.3	0.3	0.3	0
2	0.3	0.3	0.3	0.2	0.3	0.3	0.3	0.2	0.3	0.05
3	0.3	0.3	0.3	0.2	0.3	0.3	0.3	0.2	0.3	0.05
4	0.3	0.3	0.3	0.3	0.3	0.3	0.3	0.3	0.3	0

Table A3. Measurement results for surface roundness of Flank-2 after grinding. (Unit: μm)

Position of measurements	Direction of measurements	Number of measurement					Mean	Standard deviation
		1	2	3	4	5		
Root	Along involute	0.1431	0.1426	0.1412	0.1447	0.1451	0.1433	0.00159
	Along facewidth	0.0365	0.0368	0.0372	0.0378	0.0378	0.0372	0.00059
Middle	Along involute	0.1091	0.1117	0.1106	0.1105	0.1119	0.1108	0.00112
	Along facewidth	0.0331	0.0325	0.0326	0.0321	0.0327	0.0326	0.00036
Tip	Along involute	0.1135	0.1148	0.1161	0.1156	0.1163	0.1153	0.00114
	Along facewidth	0.0383	0.0377	0.0375	0.0379	0.0372	0.0377	0.00042

Table A4. Measurement results of tooth surface roundness of Flank-2 after polishing. (Unit: μm)

Position of measurements	Direction of measurements	Number of measurement					Mean	Standard deviation
		1	2	3	4	5		
Root	Along involute	0.0435	0.0438	0.0443	0.0447	0.0441	0.0441	0.00046
	Along facewidth	0.0146	0.0151	0.0149	0.0151	0.0149	0.0149	0.00021
Middle	Along involute	0.0190	0.0187	0.0193	0.0194	0.0196	0.0192	0.00035
	Along facewidth	0.0173	0.0176	0.0170	0.0171	0.0173	0.0173	0.00023
Tip	Along involute	0.0134	0.0137	0.0132	0.0135	0.0129	0.0133	0.00031
	Along facewidth	0.0255	0.0253	0.0252	0.0252	0.0256	0.0254	0.00019

References

[1] International Organization for Standardization. (2003). Gears – Evaluation of instruments for the measurement of individual gears (ISO Standard No. 18653:2003).

[2] International Organization for Standardization. (2005). Code of inspection practice – Part 5: Recommendations relative to evaluation of gear measuring instruments (ISO Standard No. ISO/TR 10064-5:2005).

[3] Frazer, R. C., Bicker, R., Cox, B., Harary, H., & Hartig, F. (2004). An international comparison of involute gear profile and helix measurement. *Metrologia*, 41(1), 12–16. https://doi.org/10.1088/0026-1394/41/1/003

[4] Kniel, K., Chanthawong, N., Eastman, N., Frazer, R., Kupko, V., Osawa, S., & Xue, Z. (2014). Supplementary comparison EURAMET.L-S24 on involute gear standards. *Metrologia*, *51*(1A), 4001. https://doi.org/10.1088/0026-1394/51/1a/04001

[5] Wang, Q., Peng, Y., Wiemann, A., Balzer, F., Stein, M., Steffens, N., & Goch, G. (2019). Improved gear metrology based on the calibration and compensation of rotary table error motions. *CIRP Annals*, *68*(1), 511–514. https://doi.org/10.1016/j.cirp.2019.04.078

[6] Wiemann, A., Stein, M., & Kniel, K. (2019). Traceable metrology for large involute gears. *Precision Engineering*, *55*, 330–338. https://doi.org/10.1016/j.precisioneng.2018.10.001

[7] Makarevich, V. (2012). Final report on supplementary comparison COOMET.L-S10: Comparison of length standards for measuring gear parameters. *Metrologia*, *49*(1A), 4004. https://doi.org/10.1088/0026-1394/49/1a/04004

[8] Kniel, K., Wedmann, A., Stein, M., Kupko, V. S., Makarevich, V. B., Lysenko, V. (2018). COOMET Supplementary comparison L-S18 (project: 673/UA-a/15). *Metrologia*, *55*(1A), 4008. https://doi.org/10.1088/0026-1394/55/1A/04008

[9] Takeoka, F., Komori, M., Kubo, A., Fujio, H., Ito, T., Takatsuji, T., & Takeda, R. (2009). High-precision measurement of an involute artefact by a rolling method and comparison between measuring instruments. *Measurement Science and Technology*, *20*(4), 45105. https://doi.org/10.1088/0957-0233/20/4/045105

[10] Taguchi, T., Ming, A., & Shimojo, M. (2011). Development of high precision gear measuring machine. *International Journal of Mechatronics and Automation*, *1*, 181–189. https://doi.org/10.1504/IJMA.2011.045250

[11] Ling, S., Lou, Z., Wang, L., & Ma, Y. (2013). Optimal forming principle and grinding experiment of the ultra-precision involute profile. *Proceedings of the Institution of Mechanical Engineers, Part B: Journal of Engineering Manufacture*, *227*(3), 375–382. https://doi.org/10.1177/0954405412469554

[12] Ferreira, N., Krah, T., Jeong, D. C., Metz, D., Kniel, K., Dietzel, A., & Haertig, F. (2014). Integration of a silicon-based microprobe into a gear measuring instrument for accurate measurement of micro gears. *Measurement Science and Technology, 25*, 0640166. https://doi.org/10.1088/0957-0233/25/6/064016

[13] Lou, Z., Wang, L., Wang, X., & Ma, Y. (2011). Measurement errors caused by radius deviation of base disc in double-disc instrument for measuring an involute. *Measurement Science and Technology*, *22*(11), 115104. https://doi.org/10.1088/0957-0233/22/11/115104

[14] International Organization for Standardization. (2013). Cylindrical gears – ISO system of flank tolerance classification- Part 1: Definitions and allowable values of deviations relevant to flanks of gear teeth (ISO Standard No. 1328-1:2013).

[15] Monier, A., Guo, B., Zhao, Q., Guo, Z., Mahmoud, T., & El-mahallawi, I. (2022). The effects of structured grinding wheel designed parameters on the geometries of ground structured surfaces. *International Journal of Advanced Manufacturing Technology*, *120*, 5551–5571. https://doi.org/10.1007/s00170-022-09048-9

[16] Heinzel, C. & Wagner, A. (2013). Fine finishing of gears with high shape accuracy. *CIRP Annals*, *62*(1), 359–362. https://doi.org/10.1016/j.cirp.2013.03.070

[17] Tanaka, K. & Koshy, P. (2019). A pneumatic sensor for grinding wheel condition monitoring. *Precision Engineering*, *56*, 62–68. https://doi.org/10.1016/j.precisioneng.2018.09.005.

[18] Ling M., Ling S., Li X., Shi Z. & Wang L. (2022). Effect on the measurement for gear involute profile caused by the error of probe position. *Measurement Science and Technology*, *33*, 115013. https://doi.org/10.1088/1361-6501/ac819f

[19] General Administration of Quality Supervision, Inspection and Quarantine of the People's Republic of China. (2016). JJF 1561-2016 Calibration specification for Gear Measuring centers.

Ming Ling received his B.Sc. degree from Xi'an University of Architecture and Technology in 2018. He is currently working toward his Ph.D. degree at Dalian University of Technology. His current research interests include precision and ultra-precision machining, precision gear grinding and measuring technology.

Siying Ling received his B.Sc., M.Sc. and Ph.D. degrees in 2004, 2007 and 2011 from Shandong Jiaotong University, Shandong University of Technology and Dalian University of Technology respectively. He is currently a professor at Shantou University. His current research interests include precision and ultra-precision machining, precision gear grinding and testing technology.

Dianqing Yu received both his B.Sc. and M.Sc. degrees in 2005 and 2008 from Northeastern University. He is now a senior engineer at Liaoning Inspection, Examination & Certification Centre. His current research interests include precision measurement of geometric quantities

Fengtao Wang received both his B.Sc. and M.Sc. degrees in 1997 and 2000 from Jilin University of Technology. In 2003 he received his Ph.D. degree from Dalian University of Technology. Now he is a professor at Shantou University. His main research interests include mechanical fault diagnosis and life prediction as well as intelligent monitoring of additive manufacturing process.

Metrol. Meas. Syst., Vol. 30 (2023), No. 4, pp. 655–673
DOI: 10.24425/mms.2023.147952

Zhihao Zhang received his B.Sc. degree from Liaoning Technical University in 2020. He is currently working toward his M.Sc. degree at Dalian University of Technology. His current research interests include precision machining and measurement technology.

Liding Wang received his B.Sc. degree in 1960 from Jilin University of Technology. He is currently a professor at Dalian University of Technology and a member of the Chinese Academy of Sciences. His current research interests include precision and ultra-precision machining, precision mechanical design, precision gear grinding and testing technology.